Resonant x-ray fluorescence holography: Three-dimensional atomic imaging in true color

S. Omori,[1,2] L. Zhao,[1,3] S. Marchesini,[1] M. A. Van Hove,[1,3,4] and C. S. Fadley[1,3]
[1]*Materials Sciences Division, Lawrence Berkeley National Laboratory, Berkeley, California 94720*
[2]*Institute of Industrial Science, University of Tokyo, Tokyo 153-8505, Japan*
[3]*Department of Physics, University of California, Davis, California 95616*
[4]*Advanced Light Source, Lawrence Berkeley National Laboratory, Berkeley, California 94720*
(Received 28 June 2001; published 5 December 2001)

We propose resonant x-ray fluorescence holography as a method for selectively imaging atoms of a specific atomic number as near neighbors around a fluorescing atom of a different atomic number. Theoretical calculations for $FeNi_3(001)$ show that the images of Ni atoms neighboring a fluorescing Fe atom can be selectively reconstructed via the differential contrasts from several holograms obtained as the incident x-ray energies are varied across the Ni *K* absorption edge. Thus, this technique should provide a unique way for determining the chemical order and disorder around a given atom, through resonant selection of its atomic number or ''true color.''

DOI: 10.1103/PhysRevB.65.014106 PACS number(s): 61.10.Dp, 61.10.Eq, 61.10.Ht, 42.40.Kw

INTRODUCTION

Following Szöke's original suggestion for inner-source x-ray fluorescence holography (XFH),[1] and some initial theoretical studies of its feasibility,[2] this technique has been experimentally developed in both normal[3] and inverse[4] modes. In the normal mode (sometimes referred to simply as XFH [Ref. 4]) modulations in the fluorescence intensity from a given atomic type as a function of emission direction are measured, yielding a hologram and permitting the three-dimensional (3D) imaging of the local environment of that particular atom. In the inverse mode (sometimes referred to as multienergy x-ray holography or MEXH [Ref. 4]) the modulation in the exciting beam intensity at a given atomic type as a function of incident direction is monitored via angle-integrated fluorescence, yielding another type of hologram. MEXH has the inherent advantage of allowing the variation of the incident energy, as long as it is above a certain absorption edge, with multienergy images being less subject to various kinds of artifacts, such as twin images and real-twin interference effects.[4] With presently available large-solid-angle detectors, MEXH is also inherently faster due to the angle-integrated signal. Recent advances in experimental technique [e.g., the high-speed ''spiral'' rotation[5] of specimens to suppress the negative effects of fluctuation in synchrotron radiation (SR) intensity] have also made it possible to obtain high quality holograms in as little as a few minutes, even though the typical modulations in either direct or inverse measurements are only a few tenths of a percent. Further theoretical studies have also been performed by several authors[6] so as to more firmly establish the fundamental basis of XFH/MEXH. From the studies to date[4,6] it is possible to conclude that a straightforward single-scattering (kinematical) model in which incoming or outgoing radiation is Thomson scattered from the various atoms in a cluster can provide a quantitatively accurate picture of XFH/MEXH effects, and that near-field effects can to first order be neglected.

Even though XFH/MEXH in its current formulation thus offers powerful methods to probe the local atomic structure around a given atom, there still remains one deficiency: the technique may be element specific for the central fluorescing atom in the structure [a quality it shares with extended x-ray absorption fine structure (EXAFS)], but there is no simple way to determine the near-neighbor atomic identities. Use can be made of the differences in x-ray-scattering strengths between different atoms (as is done with differences in electron scattering strength in EXAFS), but this is only unambiguous when atomic numbers are relatively far apart, as recently illustrated for the case of O and Ni in NiO.[7] In this paper, we propose a significant improvement to MEXH, resonant x-ray fluorescence holography (RXFH), that should enable the direct discrimination of different atoms in reconstructed images even for the most difficult cases where atomic numbers of elements involved are very close together. It is in this sense that we can speak of atomic images ''in true color.''

The principle of RXFH is discussed here for the example of a binary compound of AB_3 type with close atomic numbers, specifically $FeNi_3$ and for which $Z_{Ni}-Z_{Fe}=2$ and the fractional change in atomic number is only ~ 0.08. Prior experimental work using XFH and MEXH has already convincingly demonstrated that images of the 10–20 atoms which are within about a $(1\ \mathrm{nm})^3$ region surrounding a given atomic type can be obtained for this type of crystal with positional accuracies of 0.1–0.3 Å. Some closely related previously studied systems illustrating this are bcc Fe,[3] Cu_3Au,[4] and an AlPdMn quasicrystal.[4] Using third-generation synchrotron radiation and advanced data collection techniques has also significantly enhanced our ability to obtain such images.[5] Thus such near-neighbor positional information can be derived from a suitable multienergy dataset, as we will also demonstrate from our theoretical simulations for $FeNi_3$. However, obtaining additional information on the chemical identities in such atomic images would lead to a much more complete structural characterization of any system, particularly one in which possible compositional disorder on the nm scale is present, and thus to a much broader applicability for nanoscale materials characterization. In this study, the central atom of the reconstructed images is always chosen to be

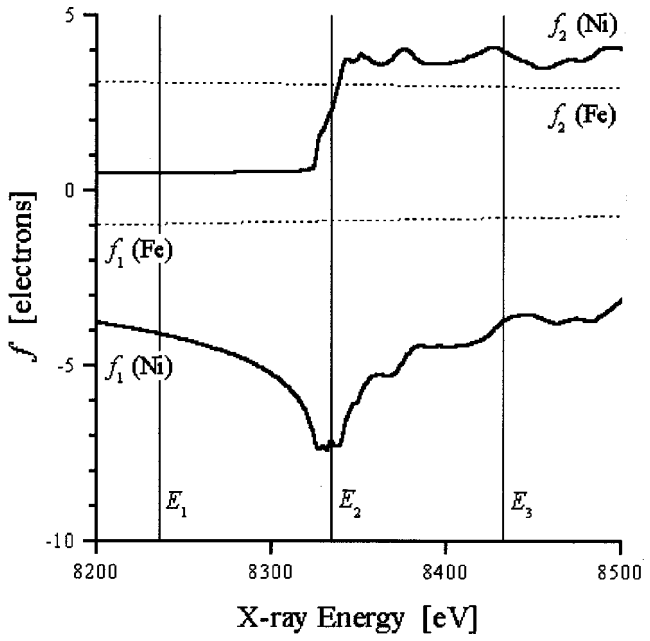

FIG. 1. The atomic x-ray-scattering factors f_1 and f_2 for Fe (dotted lines) and Ni (solid lines) as a function of x-ray energy around the K edge of Ni. The overall scattering factor is given by $f_{\mathrm{Atom}}=f_0(\theta)+f_1-if_2$, respectively. The three energies used for the simulations of E_1, E_2, and E_3 are indicated by vertical solid lines and correspond to 8235 eV ($k=4.17\,\text{Å}^{-1}$), 8334 eV ($k=4.22\,\text{Å}^{-1}$) and 8433 eV ($k=4.27\,\text{Å}^{-1}$), respectively.

atom A (Fe in this case), and the anomalous dispersion associated with an absorption edge for element B (Ni in this case) is used to selectively image atoms B surrounding the central atom. In the usual implementations of MEXH in which both atoms A and B are to be equally imaged, the incident x-ray energies E are usually chosen in such a way that they are close enough to E^A_{abs}, the absorption edge of element A, for the efficient excitation of fluorescent x rays from A, but also far enough from both E^A_{abs} and any edges E^B_{abs} of atom B that the anomalous dispersion terms in the x-ray-scattering factors for A and B are not significant. In RXFH, by contrast, we will choose several E's in the vicinity of an absorption edge E^B_{abs} of element B. The basic idea here is thus similar to that of multiple-wavelength anomalous diffraction (MAD) for phase determinations in conventional x-ray-diffraction studies,[8] but with the significant difference that there is no phase uncertainty in MEXH.

To illustrate the possible choices of excitation energy for RXFH, Fig. 1 shows the two energy-dependent parts of the x-ray scattering factors f_1 and f_2 for both elements Fe (Ref. 9) and Ni,[10] as the Ni K absorption edge at about 8334 eV is crossed. These curves are based on the best available experimental and theoretical data.[9,10] The overall scattering factor in one standard format is $f_{\mathrm{Atom}}=f_0(\theta)+f_1-if_2$, where f_0 is the atomic form factor and a function of scattering angle θ.[11] The three energies E_1, E_2, and E_3 represent choices that are within a small energy region (overall $\Delta E\approx 200$ eV) around $E^{\mathrm{Ni}}_{\mathrm{abs}}$, with E_1 "below" the edge (at least as far as the absorptive part f_2 is concerned), E_2 "at" the edge (in the sense of the maximum slope in f_2 and the maximum change in f_1), and E_3 "above" the edge (in the sense of both parts being relatively constant at post-edge values).

THEORETICAL APPROACH

Turning now to the specifics of MEXH,[4] the portions of an incident x-ray wave scattered by both the Fe and Ni atoms constitute the object waves of holography, and they interfere with the unscattered reference-wave portion to give rise to an interference field at a given Fe fluorescent emitter inside the crystal. Since all three energies are greater than the K edge of Fe, $E^{\mathrm{Fe}}_{\mathrm{abs}}=7112$ eV, the total strength of the wave field at the atomic positions for Fe can be measured by detecting Fe $K\alpha$ x rays over a solid angle that is as large as possible. Thus an inverse x-ray hologram centered on Fe can be obtained at any E near $E^{\mathrm{Ni}}_{\mathrm{abs}}$ by recording the intensity $I(k,\theta,\phi)$ of fluorescent x rays as a function of incident x-ray direction on the specimen and then normalizing I by the smooth background intensity I_0, numerically derived from I, as $\chi(k,\theta,\phi)=(I-I_0)/I_0$. From Fig. 1, we see that, as E is swept across $E^{\mathrm{Ni}}_{\mathrm{abs}}$, both components of f^{Ni}, the atomic scattering factor of Ni, change dramatically, with increments or decrements of approximately four electron units. On the other hand, the change in f^{Fe} is very small, because all absorption edges of Fe are far outside of the energy region shown in the figure (but still close enough to induce sufficiently strong Fe $K\alpha$ fluorescence for realistic experiments). Consequently, the contribution to the recorded holograms from Fe can be largely canceled out by taking the difference of two holograms at neighboring energies, while such a differential hologram can retain relatively strong contributions due to the Ni atoms as a result of the rapid change in f^{Ni} over the resonance.

To develop the holographic transform appropriate for RXFH, we begin with the mathematical expression for the differential x-ray hologram in MEXH. For illustration, the normalized hologram χ for a single emitter-scatterer pair is considered, although all of our simulations make use of calculations over large clusters of atoms, using a program developed by Len *et al.*[12] For an emitter-scatterer pair,

$$\chi(\mathbf{k})=\frac{f(k,\theta^{\mathbf{k}}_{\mathbf{R}})}{R}\exp[ikR-i\mathbf{k}\cdot\mathbf{R}]+\text{c.c.}, \tag{1}$$

where $\mathbf{k}$ is the photon wave vector, $\mathbf{R}$ is the scatterer position, $\theta^{\mathbf{k}}_{\mathbf{R}}$ is the scattering angle between $\mathbf{k}$ and $\mathbf{R}$, and $f(k,\theta^{\mathbf{k}}_{\mathbf{R}})=f_{\mathrm{Atom}}\times f_{\mathrm{Thomson}}$ includes the polarization-dependent Thomson scattering cross section. In general, $f(k,\theta^{\mathbf{k}}_{\mathbf{R}})=|f(k,\theta^{\mathbf{k}}_{\mathbf{R}})|\exp[i\varphi(k,\theta^{\mathbf{k}}_{\mathbf{R}})]\equiv|f|\exp[i\varphi]$ and so involves both a magnitude and a phase shift, and our numerical calculations allow fully for this via the quantities shown in Fig. 1. The difference of two holograms at $k_{\pm}=k\pm\delta k/2$ with $\delta k\ll k$ (as is clearly the present case) can be written in a form similar to Eq. (1), but using an effective scattering factor, as discussed recently in connection with differential photoelectron holography,[13]

$$\delta\chi(\mathbf{k})=\frac{f^{\mathrm{eff}}(k,\theta^{\mathbf{k}}_{\mathbf{R}})}{R}\exp[ikR-i\mathbf{k}\cdot\mathbf{R}]+\text{c.c.} \tag{2}$$

Here, the effective scattering factor for differential holography is

$$f^{\mathrm{eff}}(k,\theta_{\mathbf{R}}^{\mathbf{k}}) = \delta f \exp\left[i \frac{\delta k}{2}(R - \hat{\mathbf{k}}\cdot\mathbf{R}) \right] + 2if(k_-,\theta_{\mathbf{R}}^{\mathbf{k}}) \sin\left[\frac{\delta k}{2}(R - \hat{\mathbf{k}}\cdot\mathbf{R}) \right]. \quad (3)$$

Equation (3) shows two contributions to $\delta\chi$. The first is due to the change in the scattering factor $\delta f \propto \delta f_1 - i\,\delta f_2$ which can appear even for the smallest δk if there is an abrupt change in f, as at the absorption edge. The second is significant even when δf is nearly zero, as long as δk is finite. In differential photoelectron holography (DPH),[13] it has recently been demonstrated that the second term of Eq. (3) can be used to suppress the strong forward-scattering effects inherent to photoelectrons. By contrast, the first term of Eq. (3) is what we wish to emphasize in RXFH. In fact, Eq. (3) shows that $f^{\mathrm{eff}} = \delta f$ in the limit of $\delta k \to 0$, so that $\delta\chi$ in that case contains structural information only for the resonant species relative to the fluorescing atom. This suggests a first option of choosing two energies just below and just above $E_{\mathrm{abs}}^{\mathrm{Ni}}$, e.g., at $E_2 \pm \sim 8$ eV, so that the abrupt jump of the imaginary part of f^{Ni} yields $\delta f^{\mathrm{Fe}} \approx 0$ and $df^{\mathrm{Ni}} \approx -id f_2^{\mathrm{Ni}}$. We have confirmed via theoretical calculations on large clusters that this scheme works at least in principle, but we have also noted that the signal-to-noise ratio required for accurately making use of resonant effects due to δf_2^{Ni} alone is very high, if not at presently unrealistic levels. A second option which effectively amplifies the change in the real part f_1^{Ni} is thus explored here. As can be seen in Fig. 1, a larger δk range spanning E_1 to E_3 is required to fully utilize the significant change in f_1^{Ni}. As described further below, the contribution from the nonresonant atom Fe due to the second term of Eq. (3) can be greatly reduced by making use of a k sampling that has inversion symmetry with respect to the absorption edge, as is true for E_1 and E_3 in Fig. 1, which are chosen such that they equal $E_2 \pm 99$ eV.

EXPERIMENT SIMULATION AND RESULTS

For our simulations, two differential holograms, $\delta\chi_1 = \chi_2 - \chi_1$ and $\delta\chi_2 = \chi_3 - \chi_2$, have been obtained from normal holograms at the three energies shown in Fig. 1. The energy E_2 (8334 eV, $k = 4.22\ \text{Å}^{-1}$) is at $E_{\mathrm{abs}}^{\mathrm{Ni}}$ and is centered at the midpoint of the abrupt change in f_2. The energies E_1 (8235 eV, $k = 4.17\ \text{Å}^{-1}$) and E_3 (8433 eV, $k = 4.27\ \text{Å}^{-1}$) were chosen below and above E_2 with the same spacing of $\delta k = 0.05\ \text{Å}^{-1}$ relative to E_2 and a fractional change in k of only 1.1%. From the curves in Fig. 1 for Ni, it is found that $(\delta f_1^{\mathrm{Ni}}, \delta f_2^{\mathrm{Ni}}) = (-3.0, 1.7)$ and (3.5, 1.8) over $\delta\chi_1$ and $\delta\chi_2$, respectively, with units of electrons again. Since the real part of the scattering factor f_1^{Ni} decreases and increases before and after $E_{\mathrm{abs}}^{\mathrm{Ni}}$, respectively, it is beneficial to change the sign of $\delta\chi_1$ so as not to have it cancel out with $\delta\chi_2$ prior to taking a multienergy holographic transform in the usual way.[14] More precisely, we propose the transform for RXFH to be

$$U(\mathbf{r}) = \int \sigma_k k^2 dk \int \delta\chi(\mathbf{k}) \exp[i\mathbf{k}\cdot\mathbf{r}] d^2\hat{\mathbf{k}}, \quad (4)$$

where σ_k is a simple weighting factor and is $+1$ for $k > k_{\mathrm{abs}}^{\mathrm{Ni}}$ and -1 for $k < k_{\mathrm{abs}}^{\mathrm{Ni}}$, and we have here written integrals to indicate that many directions and many energies could potentially be involved. In practice, of course, these would be sums over several scanned-angle holograms at energies symmetrically placed above and below a given edge. With this choice of weighting and since the δf_2^{Ni}'s for the two differentials are nearly equal, they are canceled out in the transform of Eq. (4), and the remaining overall resonant effect due to δf_1^{Ni} is approximately 6.5 electrons. This number of electron is comparable to the normal atomic scattering factors of light elements such as C, N, and O, with the last having recently been successfully imaged by MEXH.[7] On the other hand, the contribution from Fe can be greatly reduced owing both to the opposite signs of σ_k above and below $E_{\mathrm{abs}}^{\mathrm{Ni}}$ and the very slow change in f^{Fe} with energy. It is also easy to show that, if either f or f^{eff} is real, as we are now effectively producing with our sum and weighting choice, then the real part of U has a negative peak at the atomic position.[11] Therefore we have used the negative real part of $U = -\mathrm{Re}[U]$ for presenting the reconstructed images in the following, further showing only those parts of this image function that are positive to conform to theoretical expectations: i.e., if $\mathrm{Re}[U] > 0$, image $= 0$, and if $\mathrm{Re}[U] < 0$, image $= -\mathrm{Re}[U]$. Positive-going oscillations in $\mathrm{Re}[U]$ have thus been eliminated in these images, in order to emphasize those aspects of the images that are expected based on the fundamental properties of x-ray scattering after the holographic transform.

To demonstrate the feasibility of RXFH with this approach, x-ray holograms were simulated for a model crystal of $FeNi_3$, which has the Ni fcc structure, but with all Ni atoms at the corners of the cubic unit cell replaced by Fe atoms [see octet of unit cells in Fig. 2(a)]. The lattice constant is that for the ordered phase of $FeNi_3$ (3.55 Å). The method for simulations is based on the single-scattering cluster model discussed in detail elsewhere,[12] this method has been found to be fully quantitative for describing both direct and inverse XFH data in prior work.[4,6,12] The cluster used has a spherical shape with a radius of 30 Å, and it includes a fluorescing Fe atom at the center and approximately 10 000 scatterers. The atomic form factors $f_0(\theta_{\mathbf{R}}^{\mathbf{k}})$ were calculated from standard tables.[15] The anomalous dispersion terms f_1 and f_2 for Ni shown in Fig. 1 were calculated from the experimental absorption coefficient of Ni,[10] using a computer code developed by Newville and Cross,[16] while the values for Fe were taken from another database.[9] A hologram at each of the three energies E_1, E_2, and E_3 mentioned above was calculated over the full solid angle of 4π steradians with a step width of 3° for both polar and azimuthal scans. Although is usually impossible to measure a hologram over more than about 2π steradians, for many systems such a measured hologram can be extended over the full solid angle

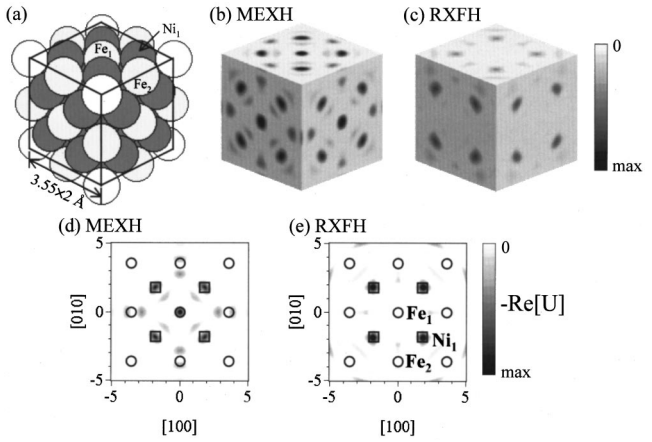

FIG. 2. Comparison of multienergy inverse x-ray fluorescence holographic images based on the negative of the real part of images generated using both the standard inversion algorithm (MEXH) and resonant holography (RXFH) via Eq. (4). These images are based on single-scattering cluster simulations of holograms at the three energies E_1, E_2, and E_3 for an $FeNi_3$ crystal containing about 10 000 atoms. (a) Near-neighbor atomic model of $FeNi_3$ for comparison to the reconstructed images in (b) and (c) and including eight unit cells with the lattice constant of 3.55 Å. Fe atoms are lighter gray, and Ni atoms darker gray. The unique types of Fe and Ni atoms observed in (b) are labeled as Fe_1, Fe_2, and Ni_1 as thin and thick gray circles, respectively, while the Fe atoms not observed in (b) are shown as open circles. (b) Three-dimensional reconstructed image from MEXH in cross section along six {001} planes. (c) Corresponding image from RXFH. The fluorescing Fe atom is located at the centers of the cubes in (a), (b), and (c). (d) Enlarged reconstructed image from MEXH in the (001) plane. (e) Corresponding enlarged image from RXFH. The true atomic positions of Fe and Ni atoms are shown as circles and squares, respectively, and certain key atomic positions are also labeled.

by using the symmetry of the crystal (e.g., inversion symmetry), with the image resolution along the vertical direction thus being improved, and resolution then in fact being nearly/fully isotropic in 3D. Our simulation thus mimics such a case. Based on a prior analysis,[12] the image resolution and the maximum radius from which the image is reliable for our choices of **k** space sampling are expected to be approximately 0.7 and 18 Å, respectively.

Three-dimensional atomic images have been reconstructed from the theoretical holograms using both the original multienergy algorithm[14] and the RXFH algorithm of Eq. (4). These images are shown in Figs. 2(b) and (c) within the cube $-3.55 \leqslant x,y,z \leqslant 3.55$ Å. Thus the length of the cube sides is twice the lattice constant of $FeNi_3$. Each image consists of six slices along the {001}-type planes, with the fluorescing Fe atom at the center of the cube, and image intensities along those planes shown in gray scale. The corresponding unit cells of the $FeNi_3$ lattice have been shown in Fig. 2(a). Five image peaks for Fe atomic sites and four image peaks for Ni sites are observed on each plane in Fig. 2(b), consistent with the expectation that such an MEXH image will be about equally sensitive to both Fe and Ni due to their cose-lying atomic numbers. Different 2D cross-section renderings over a slightly larger area are shown in Figs. 2(d) and (e). The atomic peaks for Fe denoted as Fe_2 in the figure appear to be split into two parts. Such peak splitting is often observed in single-energy holography. Even though holograms at three energies are used for the image reconstruction, the small spacing of k does not allow the complete suppression of twin images and other artifacts as in normal MEXH. Therefore, the image quality is only comparable to that of single-energy XFH. Nonetheless, all of the atomic peaks observed are fairly well resolved, and their positions are close to the true positions. In a real experimental situation, the quality of the MEXH image could be improved dramatically by using up to ten or so energies, with for example, all energies lying above both the Fe and Ni K edges. Thus, from either Fig. 2(b) or a more elaborate use of normal MEXH imaging, one can consider the atomic positions to be determinable with high accuracy, even though the atomic numbers are not as yet. On the other hand, in Fig. 2(c), using RXFH, the atomic peaks for Fe are almost completely suppressed, while the peaks for Ni are clearly visible. Figures 2(d) and (e) show even more dramatically the degree to which RXFH very effectively discriminates between two species with close atomic numbers, thus revealing the chemical order around the fluorescing atom. As a final assessment of the relative experimental difficulty of RXFH, we note that the maximum image intensity for Ni in Figs. 2(c) and (e) is approximately 18% of that in MEXH. This confirms the previous argument, based on the dispersion curve of f_1, that the experimental challenge associated with RXFH will be comparable to that with MEXH in imaging light elements such as C, N, and O. Inasmuch as the latter has recently been successful,[7] RXFH should be experimentally feasible.

CONCLUSIONS

In summary, resonant x-ray fluorescence holography (RXFH) as a method for directly determining the atomic numbers of near-neighbor atoms in a crystal has been demonstrated theoretically via single-scattering cluster calculations for $FeNi_3$ (001). To enhance the resonant effects and suppress the contributions from nonresonant species, the choice of incident x-ray energies is extremely important, and we have considered two options, one based on closely spaced energies and favoring the change in the imaginary (absorptive) part of the scattering factor and the other based on more widely spaced energies and favoring the change in the real (refractive) part. In either case, the sampling points are taken symmetrically about the absorption edge of Ni, and the modified multienergy transform of Eq. (4) was used for image reconstruction. Emphasizing the real part allows a larger δk range to be used and also enhances the overall anisotropies in differential holograms. RXFH is thus predicted to be successful in selectively imaging a single species of atoms in a compound, specifically Ni in $FeNi_3$. We expect most aspects of our analysis to apply to other combinations of A and B atoms in a given material. As a general methodology, the detailed atomic arrangement can be determined by the previously established MEXH and the chemical order and structure around each atomic type can be determined by

comparing images reconstructed via MEXH and RXFH. This combination of techniques should be particularly useful for studying such issues as the structural environment of dopant atoms in compound semiconductors, magnetic materials, and strongly correlated materials; the steepness of interfacial delta-layer profiles; and various types of phase transitions of alloys and other complex materials in which nanophase heterogeneity may be present.

ACKNOWLEDGMENTS

This work was supported in part by the Director, Office of Energy Research, Basic Energy Science, Materials Sciences Division of the U.S. Department of Energy under Contract No. DE-AC03-76SF00098. S.O. also acknowledges the support of the Japan Society for the Promotion of Science (Grant No. JSPS-RFTF 98R14101).

[1] A. Szöke, in *Short Wavelength Coherent Radiation: Generation and Applications*, AIP Conf. Proc. No. 147, edited by D. T. Attwood and J. Boker (AIP, New York, 1986), p. 361.

[2] M. Tegze and G. Faigel, Europhys. Lett. **16**, 41 (1991); P. M. Len, S. Thevuthasan, C. S. Fadley, A. P. Kaduwela, and M. A. Van Hove, Phys. Rev. B **50**, 11 275 (1994).

[3] M. Tegze and G. Faigel, Nature (London) **380**, 49 (1996); J. Kawai, K. Hayashi, T. Yamamoto, S. Hayakawa, and Y. Gohshi, Anal. Sci. **14**, 903 (1998); T. Hiort, D. V. Novikov, E. Kossel, and G. Materlik, Phys. Rev. B **61**, R830 (2000).

[4] T. Gog, P. M. Len, G. Materlik, D. Bahr, C. Sanchez-Hanke, and C. S. Fadley, Phys. Rev. Lett. **76**, 3132 (1996); D. V. Novikov, B. Adams, T. Hiort, E. Kossel, G. Materlik, R. Menk, and A. Walenta, J. Synchrotron Radiat. **5**, 315 (1998); B. Adams, D. V. Novikov, T. Hiort, G. Materlik, and E. Kossel, Phys. Rev. B **57**, 7526 (1998); K. Hayashi, T. Yamamoto, J. Kawai, M. Suzuki, S. Goto, S. Hayakawa, K. Sakurai, and Y. Gohshi, Anal. Sci. **14**, 987 (1998); M. Tegze, G. Faigel, S. Marchesini, M. Belakhovsky, and A. I. Chumakov, Phys. Rev. Lett. **82**, 4847 (1999).

[5] S. Marchesini, Ph.D. thesis, Université Joseph Fourier, Grenoble, 2000; S. Marchesini, O. Ulrich, G. Faigel, M. Tegze, M. Belakhovsky, and A. S. Simionovici, Nucl. Instrum. Methods Phys. Res. A **457**, 601 (2001); S. Marchesini *et al.*, Advanced Light Source Compendium of Abstracts (in press).

[6] P. M. Len, T. Gog, C. S. Fadley, and G. Materlik, Phys. Rev. B **55**, R3323 (1997); P. M. Len, T. Gog, D. Novikov, R. A. Eisenhower, G. Materlik, and C. S. Fadley, *ibid.* **56**, 1529 (1997); G. A. Miller and L. B. Sorensen, *ibid.* **56**, 2399 (1997); Y. Nishio and G. Materlik, *ibid.* **60**, 15 074 (1999).

[7] M. Tegze, G. Faigel, S. Marchesini, M. Belakhovsky, and O. Ulrich, Nature (London) **407**, 38 (2000).

[8] J. Karle, Int. J. Quantum Chem., Quantum Biol. Symp. **7**, 357 (1980).

[9] Center for X-Ray Optics, Lawrence Berkeley National Laboratory, Database of X-ray Optical Constants, available from http://www-cxro.lbl.gov/optical_constants/

[10] International XAFS Society Database, maintained by the Illinois Institute of Technology, and available at http://ixs.csrri.iit.edu/database/, with specific data for $FeNi_3$ at http://ixs.csrri.iit.edu/database/data/Farrel_Lytle_data/processed-data-index/

[11] D. T. Attwood, *Soft X-rays and Extreme Ultraviolet Radiation* (Cambridge University Press, Cambridge, 1999), p. 52 on our choice of sign convention for the real and imaginary parts of *f*, and p. 39 on the sign of the scattered x-ray wave field.

[12] P. M. Len, Ph.D. thesis, University of California, Davis, 1997, with program available at http://electron.lbl.gov/holopack/holopack.html

[13] S. Omori, T. Kozakai, and Y. Nihei, Surf. Rev. Lett. **6**, 1085 (1999); S. Omori, Y. Nihei, E. Rotenberg, J. D. Denlinger, S. Marchesini, S. D. Kevan, B. P. Tonner, M. A. Van Hove, and C. S. Fadley, Phys. Rev. Lett. (to be published).

[14] J. J. Barton, Phys. Rev. Lett. **67**, 3106 (1991); J. J. Barton and L. J. Terminello, in *Structure of Surfaces III*, edited by S. Y. Tong, M. A. Van Hove, X. D. Xie, and K. Takayanagi (Springer-Verlag, Berlin, 1991), p. 107; S. Y. Tong, H. Li, and H. Huang, Phys. Rev. Lett. **67**, 3102 (1991).

[15] *International Tables for X-ray Crystallography*, edited by C. H. Macgillavry, G. D. Rieck, and K. Lonsdale (Kynoch, Birmingham, 1968), Vol. III, p. 201.

[16] Consortium for Advanced Radiation Sources, Argonne National Laboratory, software from J. O. Cross and M. Newville, at http://cars9.uchicago.edu/~newville/dafs/diffkk/